

Active directional beaming by mechanical actuation of double-sided plasmonic surface gratings

Eui-Young Song,¹ Hwi Kim,^{2,*} Woo Young Choi,³ and ByoungHo Lee¹

¹National Creative Research Center for Active Plasmonics Application Systems, Inter-University Semiconductor Research Center and School of Electrical Engineering, Seoul National University, Seoul 151-774, South Korea

²Department of Electronics and Information Engineering, College of Science and Technology, Korea University, Sejong Campus, Sejong-ro 2511, Sejong 339-700, South Korea

³Department of Electronic Engineering, Sogang University, Seoul 121-742, South Korea

*Corresponding author: hwikim@korea.ac.kr

Received April 23, 2013; revised July 17, 2013; accepted August 28, 2013;
 posted August 29, 2013 (Doc. ID 189371); published September 23, 2013

A novel mechanism for active directional beaming by mechanical actuation of double-sided plasmonic surface gratings is proposed. It is shown that the asymmetric mechanical actuation of optimally designed plasmonic surface gratings surrounding a subwavelength metal slit can produce a steerable off-axis beaming effect. The controllability of the beam direction provides an opportunity to develop novel active plasmonic devices and systems. © 2013 Optical Society of America

OCIS codes: (240.6680) Surface plasmons; (250.5300) Photonic integrated circuits; (050.0050) Diffraction and gratings.

<http://dx.doi.org/10.1364/OL.38.003827>

Microscale or nanoscale directional beaming devices that can be actively controlled have been in strong demand in various fields [1]. In the field of three-dimensional (3D) displays, the generation of directional images with directional differentiation is a fundamental issue. Device-level implementation of this functionality is extremely difficult at present [2]. The development of high-speed dynamic directional light devices could produce time-sequential light field distribution to generate 3D images in space. It would also provide novel functionality for applications in photonic integrated circuits, optical communications, optical computing, optical sensing, optical manipulation of molecules, and 3D displays. Although much effort has been devoted to developing microscale static directional beaming structures [3–6], no practical active device architecture for dynamic beaming has been established yet. Research on dynamic directional beaming even at the single-pixel level on the microscale or nanoscale has been rare [1].

Recently, nanoelectromechanical systems (NEMS) technology has been emerging as one of the most powerful technologies for realizing nanoscale active photonic devices. Active metamaterials [7] and spatial light modulators [8] were fabricated based on NEMS technology.

Considering the potential application of NEMS technology to photonics, we propose a novel mechanism for a nanoscale active directional beaming device based on the mechanical actuation of double-sided plasmonic surface gratings. We show that the asymmetrically lifted double-sided plasmonic surface grating structure generates a directional beaming effect, as shown in Fig. 1.

Figure 1 illustrates the basic mechanism of directional beaming. Two diffracted beams with the same direction of radiation formed by diffraction of the leftward and rightward surface plasmon (SP) waves are spatially superposed by the surface gratings. This results in collimated directional beaming. The grating period, the dielectric thickness, and the thin-metal (Ag) layer thickness are denoted as p , t_d , and t_m , respectively. The air

gaps of the left and right surface gratings are denoted as t_L and t_R , respectively. The left and right dielectric gratings have the same permittivity but different lifting air gaps, t_L and t_R .

The directionality of the beam is determined by the air gap configuration of the double-sided surface grating, (t_L, t_R) . The effective refractive index of the grating material is the degree of freedom providing controllability of the beaming direction [6]. In [6], it was shown that the radiation angle can be changed monotonically with a linear variation in the refractive indices of the double-sided gratings. The effective refractive index of the grating material can be tuned by the air gap between the floating surface grating and the metal substrate interacting with the SP waves. The direction of the diffracted

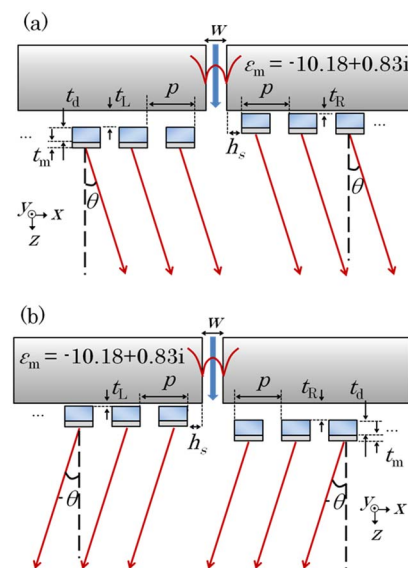


Fig. 1. Directional beaming effects by the subwavelength metal slit with double-sided plasmonic surface gratings with period p , the left and right air gaps of t_L and t_R , and the offset of h_s in cases of (a) $t_L > t_R$ and (b) $t_L < t_R$.

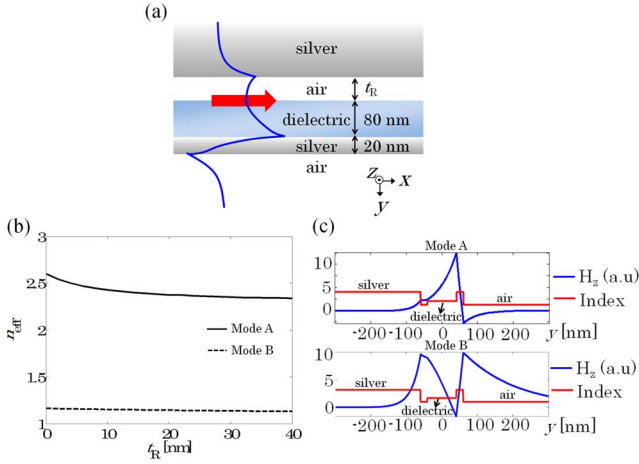


Fig. 2. (a) Schematic diagram of metal–air–dielectric–metal–air layers and SP mode propagating along the $+x$ -direction, and (b) profiles of effective indices of metal/air/dielectric/metal/air layers. There exist two SP modes (modes A and B) in the multilayer structure. (c) The magnetic field of the two modes and refractive index profiles of the multilayer structure.

beam is controlled by balancing the effective refractive indices of the left and right gratings. The right-directional and left-directional beaming effects with respect to the air gap configuration of the surface gratings (t_L, t_R) are illustrated in Figs. 1(a) and 1(b), respectively.

The floating grating can be modeled by the metal/air/dielectric/metal/air layer [9], as shown in Fig. 2(a). The effective refractive indices of the SP modes interacting with the floating grating are analyzed in Fig. 2(b). For this analysis, the thicknesses of the dielectric and the thin silver layers, t_d and t_m , are set to 80 and 20 nm, respectively. The wavelength is set to 532 nm, at which the permittivity value of silver and that of the dielectric are $-10.18 + 0.83j$ and 2.8, respectively. In Fig. 2(b), the effective refractive indices of the first and second SP modes are plotted as a function of the air gap t_r . In Fig. 2(c), the magnetic field profiles of two modes at $t_r = 20$ nm are shown. The effective refractive index of the first SP mode (mode A) is a monotonically decreasing function with respect to t_r in the range of 0–40 nm. For the air gap configurations with $t_L > t_R$ and $t_L < t_R$, it can be expected that the radiation angle would be $\theta > 0$ (deg) and $\theta < 0$ (deg), respectively. For the second SP mode (mode B), an almost constant effective refractive index ($n_{\text{eff}} = 1.2$) is extracted. The mode A propagates mainly through the lossless dielectric and thin silver layers, having a long propagation length, while the mode B is tightly confined near the metal substrate decaying fast and thus the contribution of the mode B to the beaming is negligible. Consequently, the mode A with a longer propagation length contributes to the formation of the beaming field dominantly.

To validate this idea, the optimal design parameters of the proposed structure have been found for an operating wavelength of 532 nm with the COMSOL Multiphysics simulator. The permittivity value of metal (Ag) is $10.18 + 0.83i$ at this wavelength and that of the grating dielectric material is set to 2.8. A parametric optimization process was used to decide the optimal structural parameters. The optimization goal is obtaining the best collimated

shape in the field distribution. The period ($p = 390$ nm), fill factor ($f = 0.45$), offset ($h_s = 20$ nm), dielectric thickness ($t_d = 80$ nm), and thin silver coating thickness ($t_m = 20$ nm) are set to the same values for the two gratings. The slit width w is 100 nm.

The diffraction field distribution generated by subwavelength metal slits with no gratings is visualized in Fig. 3(a). In Figs. 3(b)–3(d), directional off-axis beaming by asymmetrically lifted double-sided gratings is demonstrated. The radiation angles were estimated in the angular spectrum profile of the x -directional electric field distribution, T_x , represented in

$$E_x = \int T_x(k_x) e^{j(k_x x + \sqrt{(2\pi/\lambda)^2 - k_x^2} z)} dk_x, \quad (1)$$

where k_x is $(2\pi/\lambda) \sin \theta$ and θ is the radiation angle. In Fig. 3(e), the square of the angular spectrum profile, $|T_x|^2$, is plotted, which can be interpreted as far-field

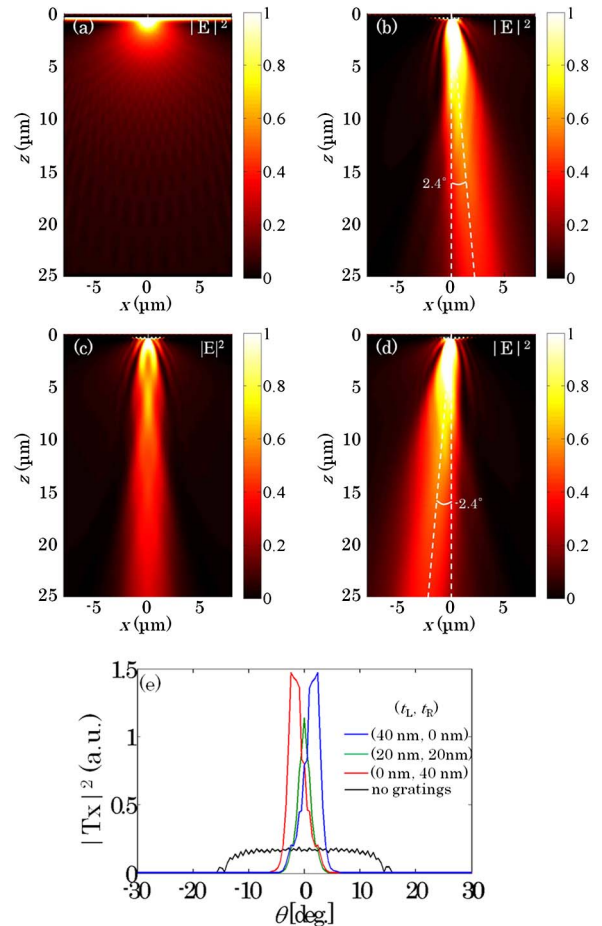


Fig. 3. (a) Diffraction field distributions generated by the subwavelength metal slits with no grating. (b) and (c) Diffraction field distributions with air gap configurations of the double-sided surface gratings for the left and right gratings of (b) $(t_L, t_R) = (40 \text{ nm}, 0 \text{ nm})$, (c) $(t_L, t_R) = (20 \text{ nm}, 20 \text{ nm})$, and (d) $(t_L, t_R) = (0 \text{ nm}, 40 \text{ nm})$. (e) Angular spectrum profiles of the diffraction fields for $(t_L, t_R) = (40 \text{ nm}, 0 \text{ nm})$ [blue], $(t_L, t_R) = (20 \text{ nm}, 20 \text{ nm})$ [green], and $(t_L, t_R) = (0 \text{ nm}, 40 \text{ nm})$ [red], which have a peak at 2.4° , 0° , and -2.4° , respectively, and that of the diffraction field from a bare slit [black].

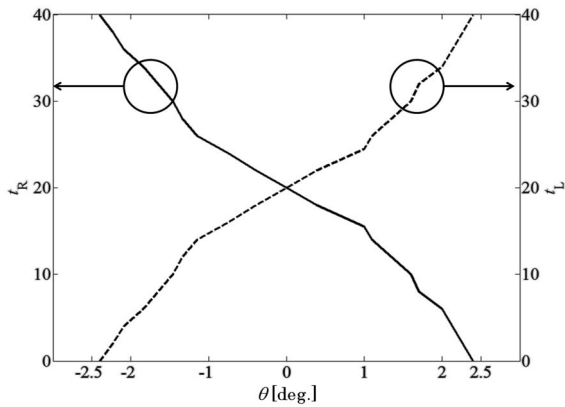


Fig. 4. Air gap configuration, (t_L, t_R) , as a function of the radiation angle of the diffracted beaming field.

pattern. The angles at the maximum peaks are extracted and determined as the radiation angles of the diffracted beams. The radiation angles in the cases of $(t_L, t_R) = (40 \text{ nm}, 0 \text{ nm})$, $(20 \text{ nm}, 20 \text{ nm})$, and $(0 \text{ nm}, 40 \text{ nm})$ are obtained as $\theta = 2.4$ (deg), $\theta = 0$ (deg), and $\theta = -2.4$ (deg), respectively. The peak intensity of the diffraction field is magnified by 7.5 times that from the bare slit by the double-sided grating.

The grating air gap configuration (t_L, t_R) is calculated as a function of the radiation angle θ in Fig. 4. The air gap variation is constrained in the range of 0–40 nm. For any specific radiation angle θ in the range of -2.4 (deg) to $+2.4$ (deg), an appropriate air gap configuration pair (t_L, t_R) can be obtained.

When the air gap is greater than 40 nm, the surface grating does not interact with the evanescent field tail of the SP wave propagating on the metal slit surface. The second SP mode presented in Fig. 2 is immune to the air gap variation, which implies that the diffraction of the second SP mode does not change with the air gap variations. The beaming effect shown in Fig. 3 is mainly ascribed to the diffraction of the first SP mode whose effective refractive index is sensitive to the air gap variation. In Fig. 3, the diffraction field components of the first and second SP modes are actually mixed. However, in the proposed structure, the coupling power of the slit to the interactive first SP mode is estimated to be greater than that to the noninteractive second SP mode, and thus the dynamic directional beaming operation is confirmed as demonstrated in Fig. 3.

In practice, the control of lifting the grating structure can be implemented using NEMS technology. An array of nanoscale clamped–clamped beams with metal electrodes at each corner is a good example [10]. A voltage will be applied between the beam and the electrode to control t_L and t_R . The central portion of the structure whose air gap thickness is adjusted electrically, sustains the surface grating structure and will be exposed to light. Calculations show that about 3.3 V is needed to actuate TiN clamped–clamped beams whose length, width, and thickness are 20, 0.1, and 30 nm, respectively, when t_L and t_R are 50 nm [10]. The air gap distance from 0 to 50 nm can be linearly controlled by adjusting the bias voltage within the 3.3 V range.

In conclusion, we have proposed a novel mechanism for NEMS-based microscale active directional that can be implemented practically. The issue of increasing the dynamic range of the beam tilting angle will be a continual focus in our research. The proposed directional beaming architecture can be further extended to various active plasmonics and display applications.

The authors acknowledge the support of the National Research Foundation and the Ministry of Education, Science and Technology of Korea through the Creative Research Initiative Program (Active Plasmonics Application Systems)

References

1. Y. Lee, K. Hoshino, A. Alu, and X. Zhang, *Opt. Express* **21**, 2748 (2013).
2. S. Reichelt, R. Häussler, G. Fütterer, N. Leister, H. Kato, N. Usukura, and Y. Kanbayashi, *Opt. Lett.* **37**, 1955 (2012).
3. T. Kosako, Y. Kadoya, and H. F. Hofmann, *Nat. Photonics* **4**, 312 (2010).
4. H. J. Lezec, A. Degiron, E. Devaux, R. A. Linke, L. Martin-Moreno, F. J. Garcia-Vidal, and T. W. Ebbesen, *Science* **297**, 820 (2002).
5. E. Ozbay, *Science* **311**, 189 (2006).
6. H. Kim, J. Park, and B. Lee, *Opt. Lett.* **34**, 2569 (2009).
7. J.-Y. Ou, E. Plum, J. Zhang, and N. I. Zheludev, *Nat. Nanotechnol.* **8**, 252 (2013).
8. K. V. Acoleyen, J. Roels, T. Claes, D. V. Thourhout, and R. Baets, in *IEEE International Conference on Group IV Photonics* (2011), p. 371.
9. J. Park, H. Kim, I.-M. Lee, S. Kim, J. Jung, and B. Lee, *Opt. Express* **16**, 16903 (2008).
10. E. S. Hung and S. D. Senturia, *J. Microelectromech. Syst.* **8**, 497 (1999).